ANALOGUE COMPUTATIONAL MODELING OF UPPER-AIRWAY DYNAMICS

G.A. Tetlow, A.D. Lucey & J. Wang
Fluid Dynamics Research Group, Curtin University of Technology, Perth, Australia.

ABSTRACT

Analogue computational models are developed and deployed to study the underlying dynamics of the human upper airway. The anatomical fluid-structure system is idealized as a cantilevered flexible plate embedded in channel flow where the lateral walls of the channel may also deform in response to fluid flow enclosed therein. When the resistances of oral and nasal inlets differ greatly, a two-dimensional study of the breathing cycle shows that the motion of the soft palate could lead to low-pressure intensification during inhalation that is a key feature of airway collapse. Studies of inhalation using the three-dimensional model show that oscillations of the soft palate have little effect on the motion of deformable side walls. However, side-wall motion strongly affects soft-plate motion and this interaction is characterized parametrically. Finally, some preliminary three-dimensional results for a breathing cycle are presented; these support the pressure-intensification mechanism hypothesized on the basis of the two-dimensional model.

1. INTRODUCTION

It has been suggested that snoring and obstructive sleep apnea (OSA) were once thought to be a defensive mechanisms scaring off predators during sleep. However, in modern society these are regarded as medical conditions for which cures or alleviation strategies are sought. Since the 1990's, mechanical models have been developed that have begun to determine the causes of these ailments as phenomena arising from flow-structure interactions; for examples, see Huang (1995), Aurégan & Depollier (1995), Guo & Paidoussis (2000) and Balint & Lucey (2005). The present paper describes our development and use of analogue computational modeling to advance understanding of the dynamics of the human upper airway. This system is particularly challenging because it comprises a flexible surface embedded in a fluid flow that itself is bounded by a channel with flexible walls. Understanding of this system will underpin the interpretation of results from geometrically more complex full anatomical models of the upper airway system that are specific to individual sufferers.

2. TWO-DIMENSIONAL MODELING

Our initial work, for example see Tetlow *et al.* (2006), focused on understanding the underlying physics of the soft palate with other channel walls (tongue and pharynx) considered rigid; a schematic of this simplified two-dimensional (2D) model is shown in Fig 1.

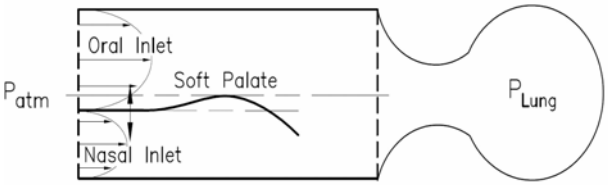

Figure 1*: Simplified geometry of the human upper airway including major anatomical features; the pressure-driven approach allows the inlet velocities to vary with airway resistance*

This analogue model of the upper airway adopted a new approach because the mean flows in the oral and nasal inlets were not prescribed. Instead they were computed as functions of the applied pressure drop and the time-varying resistances of each channel that are dependent upon the fluid-driven motion of the soft-palate. In this model, the soft palate was represented by a thin cantilevered flexible plate fully coupled to an unsteady laminar flow modeled by the 2D Navier-Stokes equations System dimensions and material properties were chosen to approximate the range that could be expected within normal anatomical variation. We modeled inhalation effort by a constant pressure drop from inlet (atmospheric conditions) to outlet (lungs). The model permits offset positions of the flexible plate within the channel to be studied correctly. This asymmetry can be used to reflect resistive differences in the nasal and oral airways. With both inlets open we showed that the well-known soft-palate flutter occurs at a sufficiently high applied pressure drop and that its mechanism is more potent for an offset plate. However, we also recognized that, at sub-critical Reynolds numbers (based on pressure drop and downstream channel height), flow-induced deformations of an offset soft plate could lead to mean-flow pressure fluctuations amplifying over the respiratory cycle; how this might occur is described herein.

We consider the case of one channel closed. This is effectively the most extreme case of resistance imbalance between the oral and nasal channels. Figure 2 shows the results of a typical inhalation when a steady applied pressure drop is applied. The lower inlet is blocked, the flow is from left to right and motion of the soft plate was initiated by deforming it into its second *in-vacuo* mode.

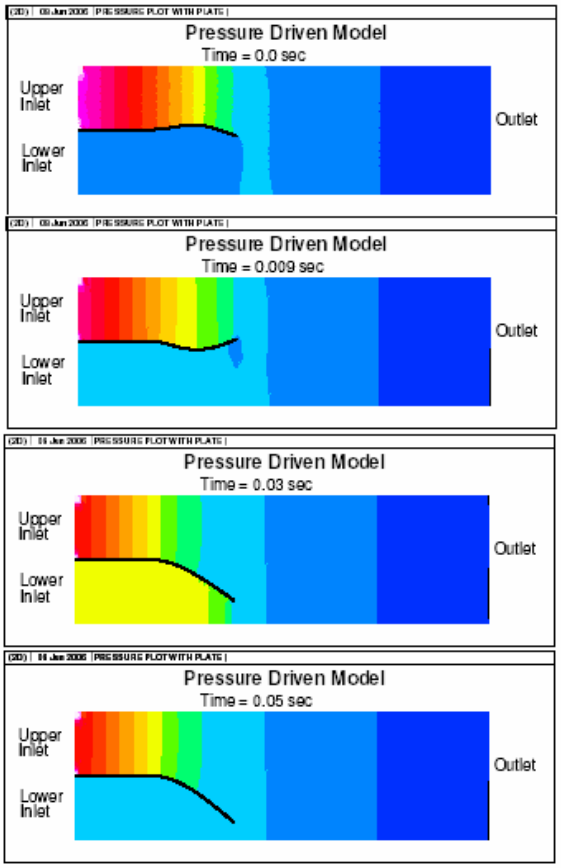

Figure 2*: Snapshots of soft-plate deflection and pressure contours (red=high to blue=low) for a typical inhalation using constant applied pressure drop and lower channel closed. Adapted from Tetlow et al. (2006)*

At early times of the simulation, oscillatory motion occurs due to the initially introduced presence of the second mode. This is damped by the fluid forcing and the plate final settles into the deformed position seen at *t=0.05* s. Note that the pressure in the closed cavity must ultimately equal that at the tip of the flexible plate.

We now investigate the exhalation phase of the breathing cycle. A constant pressure drop is applied with the lung-side pressure above atmospheric by 0.0014 N/m^2. Figure 3 shows snapshots of soft-plate position at the time at which its tip reaches its maximum vertical deflection into the open channel. The overall channel height is 5 mm high, comprising two equal channels of height 2.5 mm with the lower closed The total length of the system is 40.5 mm and the flexible plate length is 8 mm terminating in the channel 17.5 mm upstream of the lung (or right-hand) end. The flexible plate is 0.1mm thick, has an Elastic Modulus of 8800 N/m^2 and a density of 1000 kg/m^3. Air density and viscosity were respectively taken as 1.1774 kg/m^3 and 1.98 × 10^{-5} m^2/s. The simulation ran for 1.25 seconds with a time step of 5 × 10^{-5} seconds.

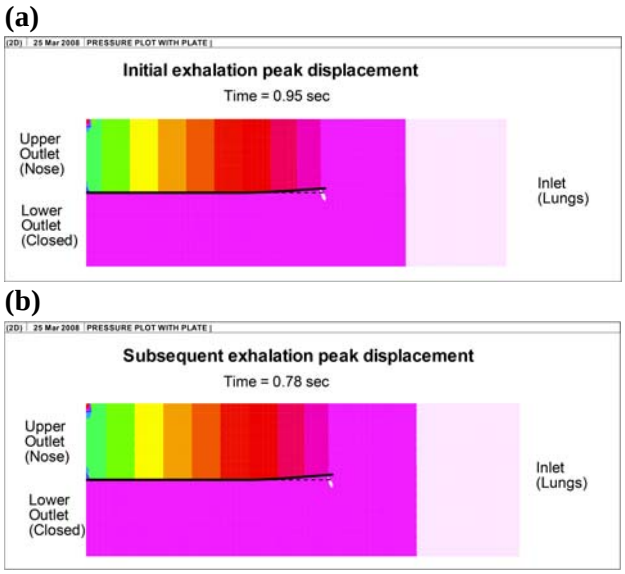

Figure 3*: Snapshots of soft-plate deflection at maximum deflection into the upper open channel during exhalation (flow from right to left) and pressure contours (light(magenta=high to orange=low); initial soft–palate position denoted by broken line, (a) undeflected and (b) the end of a previous inhalation*

The results of Fig. 3 demonstrate that during the exhalation phase, the soft palate deflects *into* the open channel, thereby *increasing its resistance* at the start of the next inhalation. This would lead to lungs applying a greater inhalatory effort to achieve a required flow rate, thereby reducing the mean pressure in the airway. Reduced pressure within the airway then heightens the risk of apenic closure of the airway due to side-wall (inward) motion. Moreover, our results show that the position of the soft palate at the start of the exhalation phase leads to differences in deflection at the start of the next inhalation; in Fig. 3b the reduction of the upper channel height due to a soft-palate tip deflection of 0.20 mm (having commenced at -0.14 mm) exceeds the 0.17 mm reached in Fig. 3a when commencing at the neutral position. This then suggests that, over a number of breathing cycles, a significant increase to the resistance of the open channel could occur. This would necessitate progressively higher levels

of lung suction during inhalation and thus a propensity to overall airway collapse. The corresponding three-dimensional effect is explored in Section 3.2 below.

3. THREE-DIMENSIONAL MODELLING

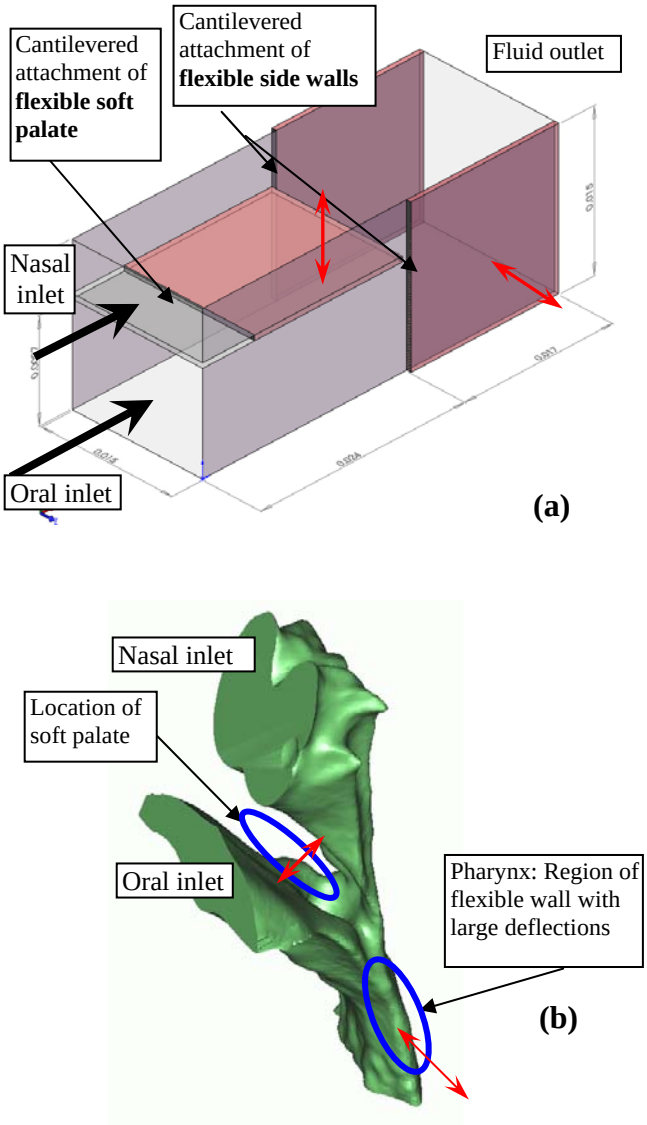

Figure 4: *Upper-airway models, (a) 3D analogue computational model, and (b) Anatomically correct reconstructed geometry (flexible regions circled). Red arrows indicate principal directions of flexible-boundary motions.*

Medical literature suggests that soft-palate motion is implicated in around 30% of OSA cases; the remainder due to collapse of the pharynx or a combination of the two. Our two-dimensional modeling suggested the linkage between the dynamics of the soft palate and pharynx. Because the motions of soft palate and pharyngeal side walls are orthogonal, we have devised a three-dimensional analogue computational model – see Fig. 4 - capable of capturing the essential dynamics while retaining simplicity and thus enabling representative phenomenology to be extracted. We solve the unsteady Navier-Stokes equations in this domain fully coupled to the mechanics of the flexible surfaces in order to conduct numerical experiments on the model flow-structure system.

The geometric configuration shown in Fig. 4a allows simple numerical modeling while the bulk sizing and material properties reflect those of the human upper airway and are similar to those used in the 2D work above. A notable departure from the real system is the representation of the pharyngeal side walls as cantilevered flexible plates. This was done to overcome the difficulty of identifying rigid connection points for the pharyngeal walls in the airway when simplifying the overall geometry from approximately elliptical. The inherent flexibility of the cantilevered arrangement permits the pharyngeal walls to collapse from the sides as clinically observed in airway narrowing and closure.

The soft palate and two flexible side walls have identical dimensions (17 x 15 x 0.5 mm) with material density 1000 kg/m^3 and Poisson ratio 0.33. The cross-section of the wholly rigid channel enclosing the upstream hard and soft palates has both width and height of 15 mm. Within this section, the hard and soft palate are offset to give lower and upper channel heights of 9.7 mm and 4.8 mm respectively (with palate thicknesses being 0.5 mm). This asymmetry represents the different calibers of the oral and nasal airways that are separated by the palate. The lengths of the hard and soft palates are 9 mm and 17 mm respectively and the overall length of the system is 41 mm. There is a three-sided fluid-structure interaction (FSI) boundary for the soft palate (upper and lower surfaces, and tip side surface) while there is just one interior FSI boundary for each side wall. Unsteady three-dimensional laminar flow is assumed, modeled by the Navier-Stokes and Continuity equations. The airflow is driven by a pressure loading, ΔP, applied across the length of the system. The external pressure is taken to be that of the inlet side.

The commercial FSI software ADINA R&D, a fully coupled finite-element solver, is used for all of the investigations reported herein. Implicit schemes have been selected to predict the motion of all of the flexible surfaces and a transient analysis for the fluid dynamics. A high-resolution preliminary simulation was first carried using 250,000 fluid tetrahedral elements and 30,000 solid brick elements. Since displacements of soft-palate tip were found to be small – see Section 3.1 below -, adaptive meshing was not needed, and thus a simpler all-brick element model could be deployed. Moreover, we were able to reduce the level of

discretisation down to 40,000 fluid plus 3,000 solid brick elements with just a 3% reduction to the accuracy of the maximum deflection of the soft palate.

3.1 Soft-palate/Pharynx interactions during inhalation

A series of numerical experiments is performed for a range of soft palate and side-wall material properties. A single applied pressure load of $\Delta P = 0.28$ N/m^2 is used throughout and the properties of air are those at 20^{0}C. The load is applied as a linear ramp function for the first 50 time steps of a numerical experiment to reach full load at 1 s. For the next 9 seconds, a further 150 time steps of size 0.06 s, at constant full load, are computed to predict the motion; thus, all time series run for 10 s.

A typical result is shown schematically in Fig. 5. The soft palate deforms upwards (*y*-displacement) and in the quantitative results that follow we track the position of Node A as being representative of soft-palate (maximum) deflection. This is reasonable since the deformation of the soft palate is overwhelmingly planar. Correspondingly, (*z*-displacement) deformation of the side-walls is represented by Node B, at mid-channel height. In this case there is non-negligible variation in the vertical direction, so choosing the mid-point records the maximum displacement. For this preliminary study, we have chosen to use a combination of pressure loading, channel dimensions and soft-palate properties that yield stable oscillatory behaviour, i.e. the mean flow speeds and Reynolds number are beneath those that would cause soft-palate flutter.

Figure 6 shows illustrative time series for the palate-tip and side-walls for the case of side-wall elastic modulus (E_w) being 200 N/m^2 with a range of soft-palate elastic modulus (E_P). It is seen throughout that the soft-palate deflects upwards into the narrower channel of greater resistance as found for the two-dimensional model while the side-walls move inwards to create a partial closure of the channel at its downstream end. Soft-palate oscillations are seen to be attenuated in these sub-critical conditions. The infinite-time result has the system arriving at a new static equilibrium position. The soft palate always comes to rest deflected into the upper, narrower, channel because there is greater flow-speed and mass flux through the lower, wider, channel that has lower resistance; see Figs. 5b and 5c. At the soft-palate tip the upper and lower channel-flows combine. A separated shear layer exists that must deflect towards the top rigid wall like the flow over a backward facing step in the extreme case of infinite upper-channel resistance. The resulting curvature of the isobars in the lower channel relative to those in the upper channel then produces a net upwards force that deflects the soft-palate. As seen in Fig. 6a, the lower the value of the soft-palate stiffness, the greater is its deflection.

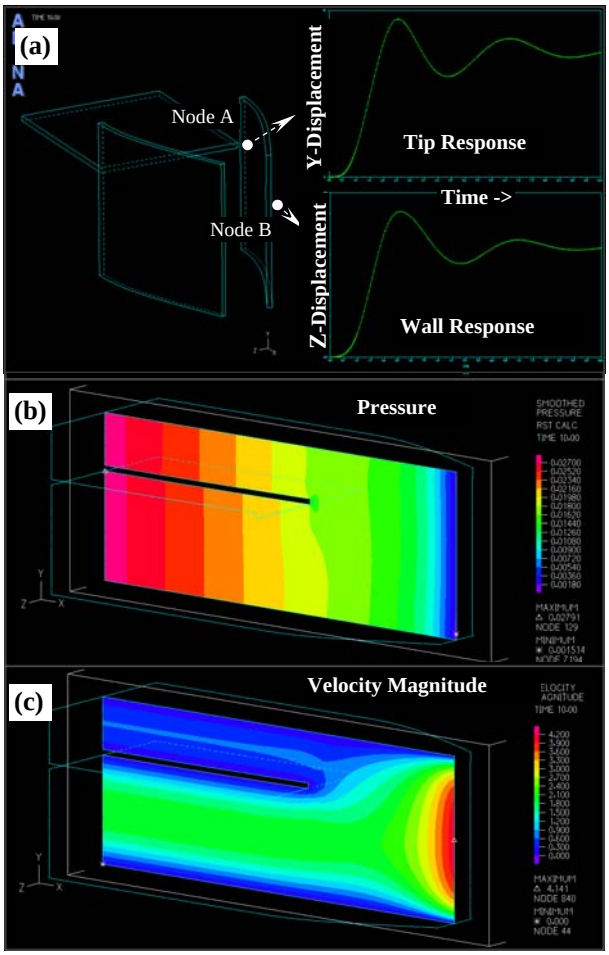

Figure 5: *Illustrative simulation of the flow-structure interaction; (a) generation of a 10-second time series and centreline flow at final equilibrium, (b) pressure contours, and (c) velocity magnitude.*

Changes to side-wall elastic modulus, $E_{W,}$ are found to generate only a small change to the final side-wall deflection – a typical response is seen in Fig. 6b - although the frequency of its pre-equilibrium oscillation is clearly dependent upon $E_{W.}$ Figure 6b serves to demonstrate that the magnitude of the soft-palate deflection has virtually no effect on the side-wall deformation. This is found to be the case throughout the range of E_W, from 200 to 2800 N/m^2, which we studied. To further confirm the insensitivity of side-wall to soft-plate deflection we artificially added uniform loads to the soft-palate, for just the first 0.5 s, that increase the amplitude of its oscillations. The soft-palate deflection asymptotes to the static deformed

states of Fig. 6a but prior to this, very large amplitudes of oscillation are observed. However, these motions have very little effect on the side-wall motion. In fact, an increase to the soft-palate amplitude by a factor of 28 results in only a maximum change of 2.8% in the amplitude of side-wall movement. This signals the insensitivity of side-wall motion to the dynamics of the soft palate and thus its behavior may be reasonably predicted by assuming a rigid soft palate when both inlet channels are open.

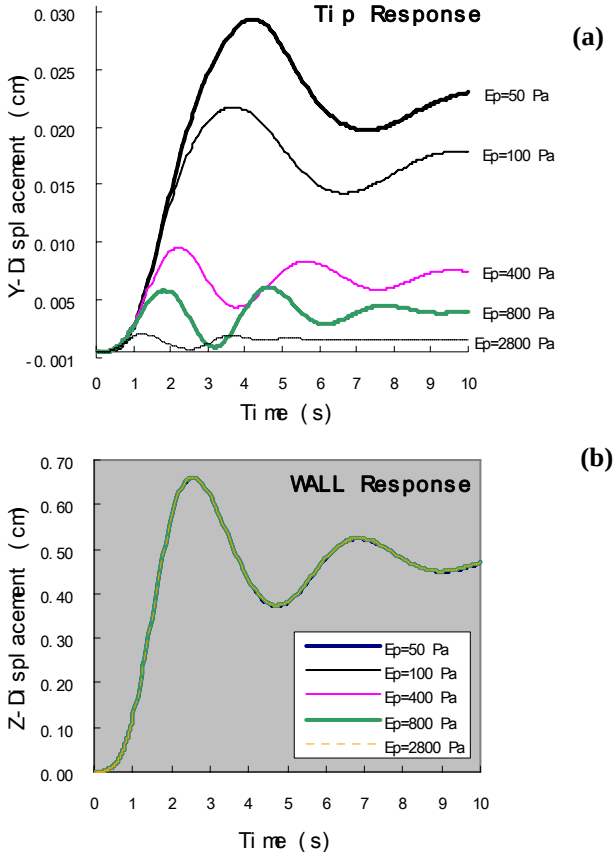

Figure 6. *Time series of (a) soft-palate tip, and (b) side-wall mid-point motion for a flexible side-wall with* E_W *=200 N/m*^{2}.

However, soft-palate behavior is strongly dependent upon both soft-palate and side-wall material properties. Three features of soft-palate response, drawn from results such as Fig 6a (and further results for other values of E_P) are used to characterize this behavior: (a) the final static-equilibrium tip deflection, (b) the peak amplitude [relative to the value of (a)] in the transient phase, and (c) the frequency of its oscillations in the transient phase. Displacements (a) and (b) are non-dimensionalised based on in-vacuo plate mechanics for which the peak deflection due to a distributed load is ($3\,\Delta P\,L^4/2E_Ph^3$) where L and h are the plate length and thickness respectively. We use ΔP on the assumption that the transmural fluid loading is directly related to the applied streamwise pressure drop across the entire channel. For a time-scale to non-dimensionalise the frequency, we use $k/(E_p)^{0.5}$ with k=1 for convenience. Figure 7 then shows the variation of the above three features for different values of E_P. While clear trends emerge, there is not total collapse of the data. This suggests that a more complex scheme is required that accounts for both solid and fluid parameters in the system. This is further suggested by a type of frequency lock-in when E_W/E_P=1 in Fig.7c and recalling that the only means of coupling is through the fluid medium.

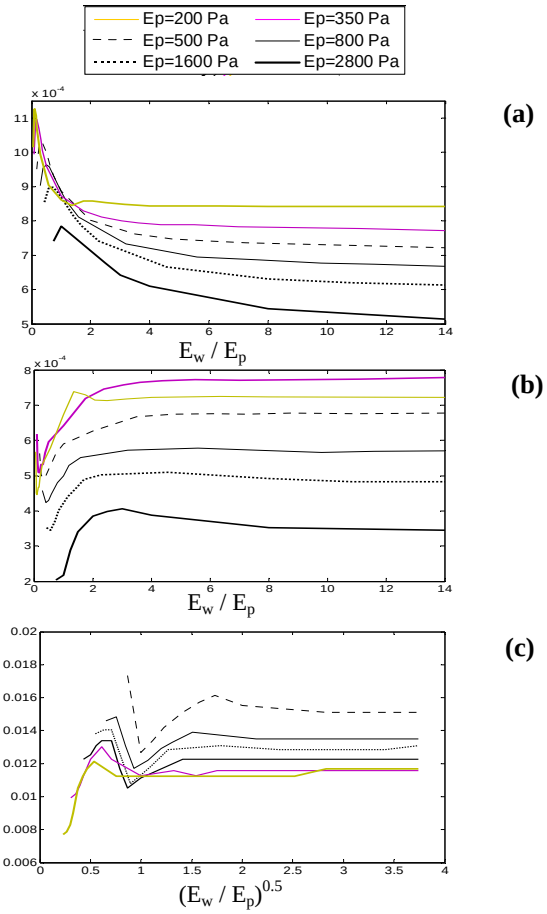

Figure 7: *Variation of non-dimensionalised soft-palate motion with side-wall stiffness: (a) final tip deflection, (b) peak amplitude of oscillation, and (c) frequency of oscillation.*

3.2 Soft-palate motions over the breathing cycle

We now present some preliminary results for the system response through part of a breathing cycle. A sequence of inhalation, exhalation, then inhalation is modeled by applying a sinusoidal variation of pressure drop across the upper airway. The period of oscillation, *T*, is set to 4 s (breathing at rest) and the pressure-drop amplitude is

$\Delta Po = 0.28$ N/m^2. The elastic moduli of the soft palate and side walls are 800 and 1600 N/m^2 respectively. The lower, wider, channel seen in Figs. 5b and 5c is closed at its left-hand end, thereby modeling nasal breathing as performed in the 2D simulations that led to Fig. 3.

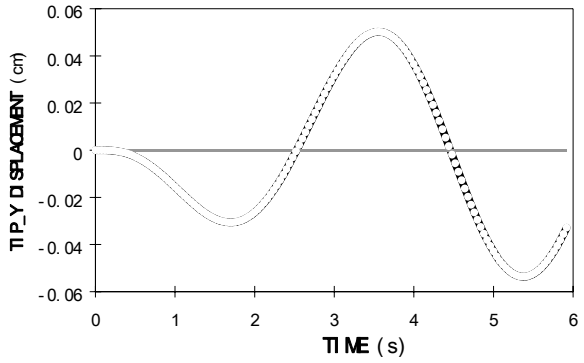

Figure 8: *Time-variation of soft-palate tip deflection through a sinusoidal sequence of inhalation-exhalation-inhalation.*

Figure 8 shows that during the initial inhalation phase, the soft palate deflects downwards into the channel of greater resistance as predicted by our 2D work above. In the following exhalation it then deflects upwards into the open channel upwards so as to increase channel – or pharyngeal - resistance. With the return to inhalation, the soft-palate moves downwards to achieve a greater amplitude than that of the first inhalation. It should be stressed that this amplification is not due to the conventional soft-palate flutter but to its interaction with a time-dependent mean flow and its coupling with the motion of the side walls. The significance of these results is that such interactions can yield an amplification of the soft-palate deflection into the open channel thereby increasing its resistance. In the anatomical system, such 'resistance-peaks' would be accompanied by increased lung suction and thus a greater likelihood of airway collapse.

4. CONCLUSION

Both two- and three-dimensional analogue computational models of the human upper-airway fluid-structure interaction system have been created. They have then been used to develop candidate explanations for the build-up of low pressure peaks in the airway over a succession of breathing cycles that could lead to collapse in an apneic event. We find that the key to such events is an imbalance between the resistances of the nasal and airway passages and its effect on palatal deflection. In the extreme case of a closed oral airway, as is frequently the case for apnea sufferers, the two-dimensional study (for an effectively rigid channel) suggests a mechanism by which the exhalation phase causes the soft palate to create a partial blockage of the open channel thereby increasing its resistance at the start of the next inhalation. This would lead to increased lung-suction effort and an overall drop in airway pressure. Over a number of breathing cycles, this effect could lead to pressure fluctuations that lead to (time-varying) periods of low pressure within the pharynx potentially sufficient to cause airway collapse. Our three-dimensional model with flexible side walls corroborates this finding and shows that side-wall motion exercises an additional strong influence on soft-palate motion that could add to the partial-blockage effect. However, we remain aware that the interactions of the two flexible components – the soft palate and pharyngeal side walls – through a time-varying mean flow could lead to some very complex flutter and resonance-type interactions within the system. Further study and characterization of these is required.

5. ACKNOWEDLEGMENTS

The authors are grateful for the support of this work by the Australian Research Council through grant DP-0559408. This work has benefited from our collaboration with Professor David Sampson (University of Western Australia) and Drs Peter Eastwood and David Hillman (Sir Charles Gairdner Hospital, Western Australia).

6. REFERENCES

Aurégan, Y. & Depollier, C. (1995) Snoring: Linear stability analysis and in-vitro experiments. *J. Sound Vib.*, **188**, pp.39-54.

Balint, T.S. & Lucey A.D. (2005) Instability of a cantilevered flexible plate in viscous two-dimensional channel flow. *J. Fluids Struct*., **20**, pp. 893-912.

Guo, C. Q. & Paidoussis, M. P. (2000) Stability of rectangular plates with free side-edges in two-dimensional inviscid channel flow. *J. Appl. Mech.* **67**, pp. 171-176.

Huang, L. (1995) Flutter of cantilevered plates in axial flow. *J. Fluids Struct.*, **9**, pp. 127-147

Tetlow, G.A., Lucey, A.D. & Balint, T.S. (2006) Instability of a cantilevered flexible plate in viscous channel flow driven by constant pressure drop. ASME Paper PVP2006-ICPVT11-93943.